View metadata, citation and similar papers at core.ac.uk

brought to you by CORE

provided by OceanRep

Changes in biogenic carbon flow in response to sea surface warming

Julia Wohlers[a,1], Anja Engel[b], Eckart Zöllner[a], Petra Breithaupt[c], Klaus Jürgens[d], Hans-Georg Hoppe[c], Ulrich Sommer[e], and Ulf Riebesell[a]

Departments of [a]Biological Oceanography, [c]Microbial Ecology, and [e]Experimental Ecology, IFM-GEOMAR Leibniz Institute of Marine Sciences, Düsternbrooker Weg 20, 24105 Kiel, Germany; [b]Department of Biological Oceanography, Alfred Wegener Institute for Polar and Marine Research, Am Handelshafen 12, 27570 Bremerhaven, Germany; and [d]Department of Biological Oceanography, Leibniz Institute for Baltic Sea Research Warnemünde, Seestrasse 15, 18119 Rostock, Germany

Edited by David M. Karl, University of Hawaii, Honolulu, HI, and approved March 9, 2009 (received for review December 18, 2008)

The pelagic ocean harbors one of the largest ecosystems on Earth. It is responsible for approximately half of global primary production, sustains worldwide fisheries, and plays an important role in the global carbon cycle. Ocean warming caused by anthropogenic climate change is already starting to impact the marine biota, with possible consequences for ocean productivity and ecosystem services. Because temperature sensitivities of marine autotrophic and heterotrophic processes differ greatly, ocean warming is expected to cause major shifts in the flow of carbon and energy through the pelagic system. Attempts to integrate such biological responses into marine ecosystem and biogeochemical models suffer from a lack of empirical data. Here, we show, using an indoor-mesocosm approach, that rising temperature accelerates respiratory consumption of organic carbon relative to autotrophic production in a natural plankton community. Increasing temperature by 2–6 °C hence decreased the biological drawdown of dissolved inorganic carbon in the surface layer by up to 31%. Moreover, warming shifted the partitioning between particulate and dissolved organic carbon toward an enhanced accumulation of dissolved compounds. In line with these findings, the loss of organic carbon through sinking was significantly reduced at elevated temperatures. The observed changes in biogenic carbon flow have the potential to reduce the transfer of primary produced organic matter to higher trophic levels, weaken the ocean's biological carbon pump, and hence provide a positive feedback to rising atmospheric CO_2.

biological feedbacks | carbon cycle | climate change | global warming | marine

The ocean plays a dominant role in the climate system through storage and transport of heat (1) and by mitigating global warming through the uptake and sequestration of anthropogenic carbon dioxide (CO_2) (2). Over the past 40 years, ≈84% of the increase in the Earth's heat budget has been absorbed by the surface oceans (3), thereby increasing the average temperature of the upper 700 m by 0.1 °C (4). This process is likely to accelerate in the next decades with a predicted increase in global mean surface temperature between 1.1 °C (low CO_2 emission scenario B1) and 6.4 °C (high CO_2 emission scenario A1FI) until the end of the 21st century (5).

Sea surface warming will affect the pelagic ecosystem in 2 ways: directly through its effect on the rates of biological processes, and indirectly through decreased surface layer mixing, causing decreased nutrient supply and increased light availability for photosynthetic organisms suspended in the upper mixed layer. It is expected that these changes in the physical and chemical environment will have drastic effects on the marine biota. The sensitivity of biological processes to temperature is commonly described by the Q_{10} factor, the factorial increase in the process rate for a 10 °C increase in temperature. While phytoplankton growth and photosynthesis show only a moderate temperature-response ($1 < Q_{10} < 2$) and are primarily controlled by incident light intensity and nutrient availability (6), bacterial heterotrophic activities typically have a Q_{10} factor between 2 and 3 (7). Moreover, bacterial growth efficiency is an inverse function of temperature, causing an increased fraction of the assimilated carbon to be respired with rising temperature (8). According to these findings, surface ocean warming is expected to shift the balance between autotrophic production and heterotrophic consumption of organic matter toward enhanced recycling and respiration. Ultimately, such alterations in the interplay of key processes involved in ocean carbon cycling may affect both pelagic food web structures and the functioning of the biological carbon pump, which transports surface-bound organic carbon to the deep ocean and hence contributes to the ocean's capacity to take up atmospheric CO_2.

To investigate the impact of rising sea surface temperature on the cycling and fate of organic carbon during a phytoplankton spring bloom, 8 mesocosms with a volume of 1,400 L each were set up in 4 temperature-controlled climate chambers. The mesocosms were simultaneously filled with unfiltered seawater from Kiel Bight (Baltic Sea) containing a natural winter/spring plankton community. The 4 climate chambers, each containing 2 replicate mesocosms, were adjusted to the following temperatures: in situ (T+0), following the natural seasonal temperature regime observed in Kiel Bight, in situ +2 °C (T+2), in situ +4 °C (T+4), and in situ +6 °C (T+6). In each of the mesocosms the build-up and decline of the spring bloom was closely monitored over 30 days.

Results and Discussion

The development of a diatom-dominated (in particular *Skeletonema costatum*) bloom was marked by an increase in chlorophyll a (Chl a) concentration (Fig. 1*A*), a rapid decline in dissolved inorganic nutrients (as shown for phosphate concentration; Fig. 1*B*), and the drawdown of dissolved inorganic carbon (DIC) caused by photosynthetic production of organic matter (Fig. 1*C*). All parameters showed an earlier onset of the bloom at elevated temperatures with an acceleration of ≈1 day/°C. While maximum Chl a concentration and nutrient consumption did not differ significantly between treatments, a distinct effect of temperature on the uptake of DIC was observed (Fig. 2). Here, elevated temperatures led to a significant decline in the maximum net consumption of DIC (ΔDIC_{max}) (Fig. 2*C*; $P = 0.014$) (see *Materials and Methods* for details on calcula-

Author contributions: A.E., K.J., H.-G.H., U.S., and U.R. designed research; J.W., E.Z., and P.B. performed research; J.W. and P.B. analyzed data; and J.W., A.E., E.Z., K.J., and U.R. wrote the paper.

The authors declare no conflict of interest.

This article is a PNAS Direct Submission.

[1]To whom correspondence should be addressed. E-mail: jwohlers@ifm-geomar.de.

This article contains supporting information online at www.pnas.org/cgi/content/full/0812743106/DCSupplemental.

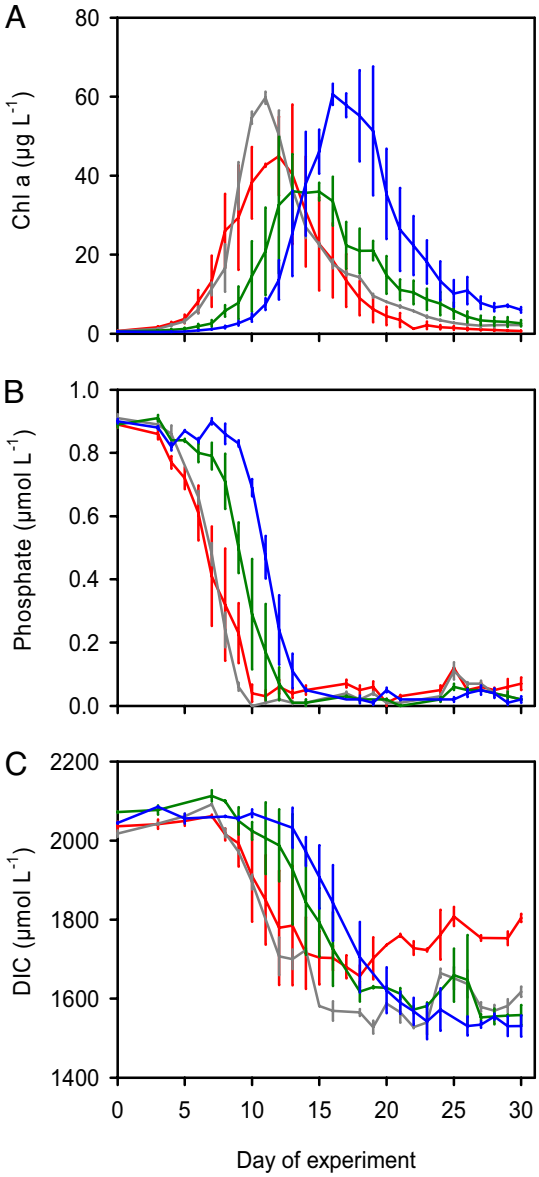

Fig. 1. Temporal bloom development. Concentrations of Chl a (*A*), dissolved inorganic phosphate (PO_4^{3-}) (*B*), and DIC (*C*). The different colors represent the 4 temperature regimes: in situ temperature T+0 (blue) and elevated temperatures T+2 (green), T+4 (gray), and T+6 (red). Solid lines denote the average of 2 replicate mesocosms. Error bars indicate the range of the replicates.

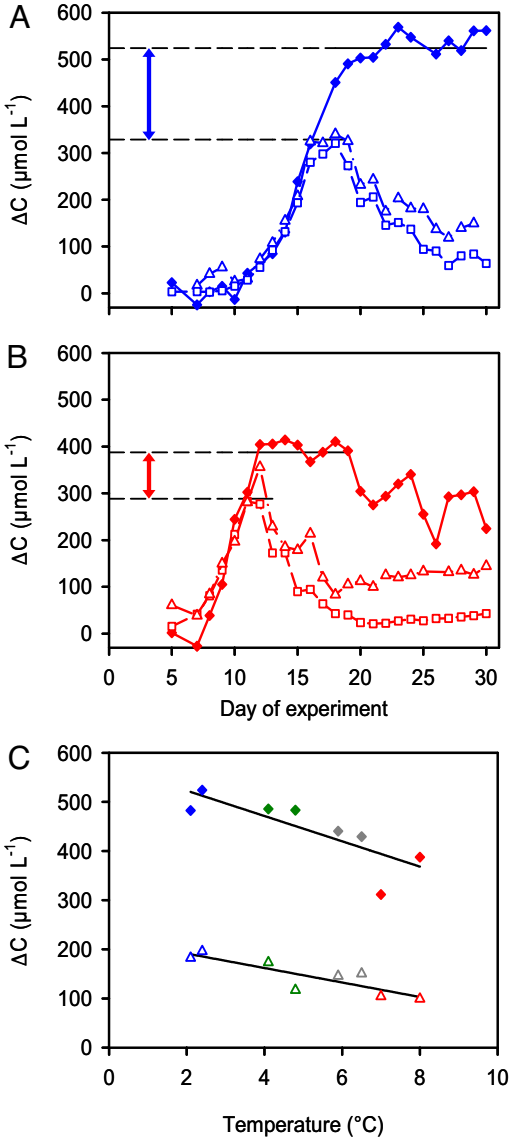

Fig. 2. Temperature sensitivity of inorganic carbon consumption, organic carbon build-up and loss. (*A* and *B*) Temporal development of the net draw-down of DIC (ΔDIC; ◆/solid line), the net build-up of POC (ΔPOC; □/dashed line), and the net build-up of TOC (ΔTOC = ΔPOC + ΔDOC; △/dashed-dotted line) at in situ temperature T+0 (*A*, blue) and at elevated temperature T+6 (*B*, red) (data from 1 replicate mesocosm of each treatment). The 2 horizontal lines in each panel indicate the magnitude of the maximum net consumption of DIC (ΔDIC_{max}, upper line) and the maximum net build-up of TOC (ΔTOC_{max}, lower line); the arrow indicates the magnitude of the net loss of organic carbon from the water column (ΔC_{loss}) at the time of maximum organic carbon accumulation. (*C*) ΔDIC_{max} (◆) and ΔC_{loss} (△) as a function of temperature. Color code is as in Fig. 1. Solid lines denote linear regressions ($n = 8$; ΔDIC_{max}: $R^2 = 0.66$, $P = 0.014$; ΔC_{loss}: $R^2 = 0.74$, $P = 0.006$).

tions), yielding an average difference of 153 μmol C·L^{-1} between the in situ treatment (T+0) and the warmest treatment (T+6).

The photosynthetic uptake of DIC was accompanied by a rapid build-up of particulate organic carbon (POC) and a gradual accumulation of dissolved organic carbon (DOC) (Fig. S1). In contrast to the observed temperature effect on DIC drawdown, the maximum net build-up of both POC (ΔPOC; Fig. 2*A* and *B*) and suspended total organic carbon (TOC) (ΔTOC = ΔPOC + ΔDOC; Fig. 2 *A* and *B*) was not markedly affected by changes in temperature. Yet, immediately after the biomass peak an enhanced accumulation of DOC occurred at elevated temperatures, indicating a pronounced shift in the partitioning of organic matter between the dissolved and particulate pool.

In all treatments, the photosynthetic draw-down of DIC exceeded the build-up of suspended organic carbon, revealing the presence of an additional carbon sink. This loss of organic carbon (ΔC_{loss}) from the water column, calculated as the difference between ΔDIC_{max} and the maximum net build-up of TOC ($\Delta C_{loss} = \Delta DIC_{max} - \Delta TOC_{max}$), showed a significant decline with increasing temperature (Fig. 2*C*; $P = 0.006$), resulting in an up to 46% lower loss at T+6 compared with the in situ temperature. Although in principle 3 processes may account for the loss of carbon from the water column (i.e., CO_2 outgassing, organic carbon fixation through algal growth on mesocosm walls, and sinking of organic matter), there is reasonable evidence that bottom accumulation of organic matter through sinking was the predominant loss term (see also *SI Text*).

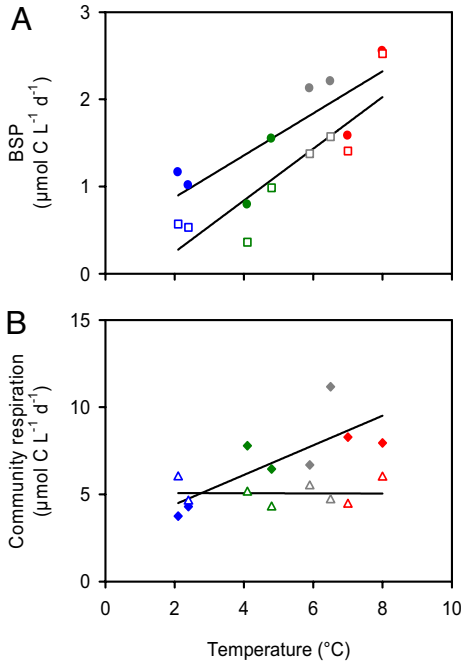

Fig. 3. Temperature dependency of BSP and CR rates at the time of maximum organic carbon accumulation. (*A*) BSP of free-living bacteria (<3 μm), as measured by ^{3}H-leucine (BSP$_{leu}$; ●) and ^{3}H-thymidine incorporation (BSP$_{thy}$; □). (*B*) CR in the bacterial (CR <3 μm; △) and nonbacterial (CR >3 μm; ◆) size fractions. Color code is as in Fig. 1. Solid lines denote linear regressions (n = 8; BSP$_{leu}$: R^2 = 0.68, P = 0.012; BSP$_{thy}$: R^2 = 0.79, P = 0.003; CR <3 μm: R^2 = 0.0002, P = 0.98; CR >3 μm: R^2 = 0.60, P = 0.025).

The combination of the observed responses to rising temperature, namely the decrease in both net inorganic carbon consumption (ΔDIC_{max}) and net loss of organic carbon from the water column (ΔC_{loss}), poses questions regarding the underlying mechanisms. Although the decline in ΔDIC_{max} with rising temperature could have resulted from a reduction in photosynthetic carbon fixation, this idea is neither supported by ^{14}C primary production measurements (see also *SI Text* and Fig. S2) nor data on phytoplankton biomass, as indicated by Chl a concentrations (Fig. 1*A*). Alternatively, this inverse relationship of ΔDIC_{max} with temperature may have been caused by enhanced heterotrophic recycling and respiration of primary produced organic matter, thereby replenishing the DIC pool and reducing the availability of organic carbon for export processes. This notion, in fact, is supported by data on bacterial secondary production (BSP), showing an earlier increase in and higher maxima of production rates at elevated temperatures (Fig. S3*A*). Thus, at the time of maximum organic carbon accumulation BSP rates of free-living bacteria significantly increased by a factor of 2–3 between the in situ temperature and T+6, both in terms of protein production (^{3}H-leucine incorporation) and cell production (^{3}H-thymidine incorporation) (Fig. 3*A*; BSP$_{leu}$: P = 0.012; BSP$_{thy}$: P = 0.003). This pattern was driven by an increase in the abundance of bacterial cells and in cell-specific BSP rates with, for instance, BSP$_{thy}$ values rising from 0.4 ± 0.01 pmol C·cell^{-1}·d^{-1} at in situ temperature to 0.99 ± 0.19 pmol C cell^{-1}·d^{-1} in the T+6 treatments. Compared with the activities of free-living bacteria at the time of maximum biomass accumulation (e.g., BSP$_{thy}$: 0.4–2.5 μmol C·L^{-1}·d^{-1}; see Fig. 3*A*), particle-associated bacteria were only of minor importance for carbon turnover as their BSP rates were markedly lower (e.g., BSP$_{thy}$: 0.08–0.17 μmol C·L^{-1}·d^{-1}).

Size-fractionated respiration measurements indicate that the bacterially-consumed organic carbon was not immediately respired, because community respiration (CR) in the <3-μm fraction remained low and apparently unaffected by temperature (Fig. 3*B*; P = 0.98). Instead, it is the respiration in the fraction >3 μm that responded positively to warming. A comparison of respiration rates in this larger-size fraction at the time of maximum organic carbon accumulation revealed a significant, 2-fold increase in daily organic carbon consumption with rising temperature (Fig. 3*B*; P = 0.025), ranging from 4.0 ± 0.3 μmol C·L^{-1}·d^{-1} at in situ temperature to 8.1 ± 0.2 μmol C·L^{-1}·d^{-1} at T+6. Most likely, this signal results both from enhanced transfer of bacterial carbon to higher trophic levels (e.g., through protist grazing) and increased algal respiration at elevated temperatures.

The pronounced response of respiratory processes to rising temperature also became apparent in the postbloom phase. Here, DIC concentrations started to increase again in the T+6 treatments by on average 115 ± 31 μmol C·L^{-1} (Fig. 2*B*), whereas they remained unaffected at in situ temperature until the end of the experiment (Fig. 2*A*). Because it cannot be ruled out that degradation of organic matter accumulating at the bottom of the mesocosms during the postbloom phase contributed to the respiratory signal in the water column, this phase was not considered in any of the calculations given above.

Another process that showed a response to elevated temperatures was the aggregation of organic matter. The concentration of transparent exopolymer particles (TEP) increased considerably in the warmest treatment T+6 and to a lesser extent also in the T+4 treatment during the postbloom phase of the experiment, whereas it remained low at T+2 and T+0 (see also *SI Text* and Fig. S4). Elevated temperature also stimulated TEP production (9) and aggregation of organic matter (10) in incubations of monoalgal cultures. The potential of TEP to promote aggregation and sinking of particulate matter has been shown in both mesocosm studies (11) and field studies (12). The extent to which enhanced TEP formation could affect particle sinking in a warming ocean critically depends on the timing of TEP production and the interplay with other biological processes, e.g., microbial degradation and grazing. In our experiment, particulate matter concentrations had decreased to nearly prebloom levels when TEP concentrations increased, hence limiting the potential for TEP-mediated particle export.

Combining the observed temperature sensitivities in a chart of processes driving surface layer carbon flow illustrates 1 piece of the complex puzzle of biological responses to ocean warming (Fig. 4). In line with theoretical considerations, our study provides evidence for a temperature-induced shift in the balance between autotrophic production and heterotrophic consumption of organic matter. At elevated temperatures enhanced respiratory loss and recycling of organic carbon become effective already during the build-up of the phytoplankton bloom. As a result, for the same amount of nutrient drawdown, the net DIC consumption decreases significantly with rising temperature. In addition, the proportion of primary produced organic matter channeled into DOC, most notably after nutrient exhaustion, strongly increases with rising temperature. Apparently the enhanced bacterial activity at elevated temperatures could not prevent this increase in DOC accumulation, suggesting that dissolved organic matter (DOM) degradation may have been limited by nutrient availability (13). However, it has been reported that the bacterial breakdown of organic matter through the action of exoenzymes can lead to the production and release of more refractory dissolved organic compounds (14). Thus, a stronger bacterial activity may, in fact, even contribute to the accumulation of DOC.

In concert, the observed temperature effects, in particular the enhanced rate of POC degradation and alterations in the partitioning of organic carbon, reflect a shift in food web structure increasing the flow of organic matter through the microbial loop (Fig. 4). This shift has the potential to reduce both

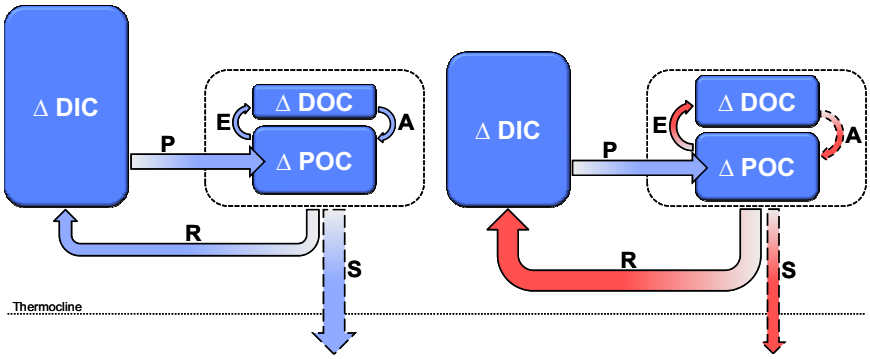

Fig. 4. A schematic illustrating the surface layer carbon flow during an algal spring bloom under present (*Left*) and elevated (*Right*) sea surface temperature. Boxes (ΔDIC, ΔPOC, ΔDOC) represent the change in the respective reservoir over time, arrows depict processes (P = primary production, E = exudation, R = respiration, S = sinking, A = aggregation). Processes found to be sensitive to warming in this study are marked in red. According to our findings, rising sea surface temperature leads to enhanced respiratory consumption of organic carbon relative to autotrophic production, already occurring during the build-up of the spring bloom. This results in a decline in net DIC consumption (ΔDIC) and a lowered availability of organic carbon for export processes. Additionally, the partitioning of organic carbon between the dissolved and particulate pools is affected, with enhanced accumulation of dissolved organic matter. Together, these changes in biogenic carbon flow have the potential to alter the efficiency of the biological carbon pump.

the transfer of organic matter and energy to higher trophic levels and the efficiency of the biological carbon pump in sequestering carbon from the surface ocean to depth, with far-reaching implications for the sustainability of global fisheries and the ocean's mitigating effect on anthropogenic climate change.

In a changing future ocean, direct effects of rising sea surface temperature, as observed here, will interact with indirect effects via increased surface layer stratification, leading to higher light availability and reduced nutrient supply. The interplay of these effects is likely to exert the strongest impact in temperate and high latitude regions. These are characterized by a seasonally high availability of nutrients caused by deep winter-mixing and include some of the most productive ocean areas. Spring blooms, as investigated in this study, are a dominant feature in the seasonal cycle of these systems, caused by a temporal decoupling of autotrophic and heterotrophic processes due to a stronger temperature limitation of the latter. The fate of the organic matter accumulating during these events is largely controlled by zooplankton grazing and export below the winter-mixed layer. In a warming ocean, the interplay of reduced nutrient supply with shifts in food web structure and a more rapid cycling of organic matter and nutrients through the microbial loop, as reminiscent of the oligotrophic ocean provinces at lower latitudes, will likely reduce both the transfer to higher trophic levels and the export potential in these areas.

Our findings are consistent with model results (15) suggesting that especially the productive parts of the ocean may be sensitive to sea surface warming in terms of organic matter export. The model shows that in areas of moderate to high productivity the ratio of export production to total primary production (i.e., the ef-ratio) is controlled mainly by and negatively correlated with temperature. At temperatures <20 °C a steep transition from high to low ef-ratios occurs as the productivity of the system declines. Thus, the interaction of direct and indirect effects of rising sea surface temperature may shift mid- to high-latitude ocean areas from high to low ef-modes and significantly reduce global carbon export.

In addition to sea surface warming, CO_2-induced ocean acidification and its effects on planktonic calcification (16–18) and primary production (e.g., ref. 19) will further complicate the picture. Together, these changes in the physical and chemical environment may, aside from their impact on biogeochemical cycling, also modify pelagic ecosystem functioning, for instance through shifts in the abundance and biogeographical distribution of key species or in the phenological coupling of different trophic levels ("match—mismatch") (e.g., refs. 20–25). Surface-ocean warming is therefore bound to be one of the most powerful drivers for future changes in ocean productivity, biogeochemical cycling, and air-sea CO_2 exchange. To project the impacts of these changes on marine ecosystem services and the climate system it is imperative that we gain a quantitative understanding of the underlying processes. These are presently not well constrained, partly because of the lack of data providing an integrated representation of upper-ocean, biotically-driven processes, and partly because of the lack of realistic biological simulations in Atmosphere Ocean General Circulation (AOGC) modeling. Understanding the full suite of interrelated responses and predicting their impacts on ecosystem dynamics, biogeochemical cycling, and feedbacks to the climate system requires a multidisciplinary effort of seagoing and experimental marine scientists in concert with modelers covering the range from ecosystem to AOGC modeling.

Materials and Methods

Experimental Set-Up. The indoor-mesocosm study was conducted between January 6 and February 5, 2006 at the Leibniz Institute of Marine Sciences. Eight mesocosms with a volume of 1,400 L were set up in 4 temperature-controlled climate chambers and filled with unfiltered seawater from Kiel Fjord (Western Baltic Sea) containing a natural winter/spring plankton community. Mesozooplankton was added from net catches in natural overwintering densities of $\approx$10 individuals L^{-1}. The temperature of the 4 climate chambers was adjusted to 2.5 °C, 4.5 °C, 6.5 °C, and 8.5 °C, respectively. The lowest temperature of 2.5 °C (in situ treatment T+0) was derived from a 10-year (1993–2002) meteorological database for Kiel Bight. The elevated temperature regimes, in situ +2 °C (T+2), in situ +4 °C (T+4), and in situ +6 °C (T+6), were chosen according to the projected increase in surface temperature of 4–10 °C during winter in the Baltic Sea region (based on AOGCM climate model simulations as summarized in ref. 26). Light was supplied by a computer-controlled illumination system, generating a diurnal triangular light curve with maximum light intensities at midday and an overall 12:12-h light/dark cycle (see also Table S1). The illumination system contained full-spectrum light tubes [10× JBL T5 Solar Tropic (4,000 K), 2× JBL T5 Solar Natur (9,000 K)], which covered the full range of photosynthetically-active radiation (PAR; 400–700 nm). Based on the light measurements at midday, a daily photon flux of 1.93 mol photons·m^{-2}·d^{-1} was calculated for the mesocosms (see *Calculations* section). This value compares well with latitudinal-averaged community compensation irradiances of 0.9–1.75 mol photons·m^{-2}·d^{-1} estimated to generate the initiation of the North Atlantic spring bloom (27). Initial concentrations of dissolved inorganic nutrients were 0.9 μM phosphate (PO_4^{3-}), 8 μM nitrate (NO_3^-), 5.6 μM ammonium (NH_4^+), and 20.4 μM silicate ($Si(OH)_4$). Because of the unusually low NO_3^- concentration in this year, another 13 μM NO_3^- was added to ensure bloom development. The water

body was gently mixed with a propeller attached to the side of the mesocosm. With this, cells and smaller particles were kept in suspension, while larger particles and aggregates forming during the bloom sank out of the water column. Water samples were taken daily with a silicon hose from intermediate depth. After addition of nutrients and mesozooplankton, we followed the build-up and decline of the phytoplankton bloom over 30 days.

Measurements. Temperature, salinity, and pH were measured three times per week with a WTW conductivity/pH probe. The maximum light intensity at midday was measured 5 times per week with a submersible 4π-PAR sensor (LiCOR) in a water depth of $\approx$10 cm. Samples for dissolved inorganic nitrate, nitrite, phosphate, and silicate were prefiltered through 5-μm cellulose acetate filters and measured with an autoanalyzer (AA II) (28). Ammonium was determined from unfiltered water samples (29). DIC was measured on sterile-filtered samples via coulometric titration (30). Total alkalinity was determined from $HgCl_2$-poisoned samples by using the Gran electrotitration method (31). Samples for the analysis of Chl a were filtered onto glass fiber filters (GF/F; Whatman) and stored at -20 °C. Pigments were extracted in 90% acetone and measured on a 10-AU Turner fluorometer (32). For the determination of POC, samples were filtered onto precombusted (5 h, 450 °C) GF/F and stored at -20 °C until analysis. Filters were dried for 6 h at 60 °C and analyzed on a Eurovector EuroEA-3000 elemental analyzer (33). Samples for DOC were filtered through precombusted GF/Fs. The filtrate was collected in precombusted (12 h, 450 °C) glass vials and stored at -20 °C. The analysis was carried out on a Shimadzu TOC_{VCN} by using the HTCO method (34). BSP was assessed by measuring the incorporation of ^{3}H-leucine (^{3}H-leu; indicator for protein synthesis) and ^{3}H-methyl-thymidine (^{3}H-thy; indicator for DNA synthesis) (35, 36). ^{3}H-leu (specific activity: 160 μCi·nmol^{-1}) and ^{3}H-thy (specific activity: 63 μCi·nmol^{-1}) were added to the samples at final concentrations of 103 nmol·L^{-1} and 8 nmol·L^{-1}, respectively. The samples were dark-incubated at in situ temperature (i.e., in the respective climate chambers) for 1.5–3 h. Incubation was terminated by adding formaldehyde (1% vol/vol). To distinguish between total and particle-associated carbon production, 5 mL of sample was filtered onto 0.2- and 3-μm polycarbonate membrane filters (Poretics), respectively. The filters were subsequently rinsed with ice-cold 5% TCA solution before being radio-assayed in 4 mL of scintillation mixture (Lumagel Plus) on a Packard TriCarb scintillation counter. All incubations were carried out in triplicate. A formalin-killed sample was used to correct for background absorption of radioactivity. To convert the incorporation of ^{3}H-leu and ^{3}H-thy into carbon production (μg C L^{-1}·h^{-1}), a theoretical conversion factor of 3.1 kg C·mol^{-1} leucine (35) and an empirically-determined conversion factor of 30.87 kg C·mol^{-1} thymidine (P. Breithaupt, personal communication), respectively, were used. The daily carbon production rates (μmol C·L^{-1}·d^{-1}) were then calculated, assuming that bacterial production rates were constant throughout the day. CR was determined by using the Winkler titration method with automated photometrical end-point detection. To distinguish between total CR and bacterial respiration (CR $<$3 μm), half of the samples were gently filtered ($<$ 200 mbar) through 3-μm polycarbonate filters before the incubation. Samples were dark-incubated at in situ temperature for 48 h. All incubations were carried out in triplicate. To calculate respiratory C utilization (μg C·L^{-1}·h^{-1}), respiration in terms of O_2 uptake (mg·L^{-1}·h^{-1}) was multiplied with a factor of 0.32 as determined for marine substrates (37). Daily respiration rates (μmol C·L^{-1}·d^{-1}) were then calculated, assuming that respiration rates remained constant throughout the day.

Calculations. ***Air-sea exchange of CO_2.*** DIC concentrations were corrected for CO_2 gas exchange between mesocosm water and atmosphere following the approach described in ref. 38, including a chemical enhancement factor (39).
Net consumption of DIC (ΔDIC), and net build-up of POC (ΔPOC) and DOC (ΔDOC). For each mesocosm, the first 2 days of sampling were set as the baseline for all calculations, because they were not significantly affected by any biological activities. For the determination of ΔDIC, each data point was subtracted from this baseline value. In the case of ΔPOC and ΔDOC, the baseline value was subtracted from the respective data point to yield the net organic carbon production.
Maximum net consumption of DIC (ΔDIC_{max}). ΔDIC_{max} was calculated from the difference between the initial (DIC_i) and the minimum DIC concentration (DIC_{min}): $\Delta DIC_{max} = DIC_i - DIC_{min}$. DIC_{min} was calculated as the mean of DIC concentrations measured after the period of exponential bloom development. For this, the natural logarithm (ln) of DIC measurements was plotted against time. During the period of exponential phytoplankton growth ln [DIC] scaled linearly with time. The first data point deviating from the linear regression was the first to be included in the calculation of DIC_{min}. In the T+0 and T+2 treatments [DIC] stabilized thereafter. Hence in these cases, all DIC measurements after the period of exponential growth were included in the calculation of DIC_{min}.

In the T+4 and T+6 treatments [DIC] started to increase again because of respiratory processes after a short stagnant period. Here, DIC_{min} was calculated from measurements obtained after exponential growth and before the subsequent increase in [DIC]. Data points used for calculating DIC_{min} are marked by a solid black line in Fig. 2 *A* and B.
Net organic carbon loss (ΔC_{loss}). For reasons of comparability, ΔC_{loss} was calculated for each mesocosm at the time of maximum biomass. It is defined as the difference between ΔDIC_{max} and the maximum net build-up of TOC (ΔTOC_{max}) with $\Delta TOC = \Delta POC + \Delta DOC$. ΔTOC_{max} was calculated as the average of 3 consecutive days (the day with the highest biomass concentration and 1 day before and after).
BSP and CR at the time of maximum biomass accumulation. The given rates represent mean values of measurements obtained right before and after the biomass peak (i.e., 1–3 days).
Daily photon flux. Based on the average maximum light intensity of 179.6 μmol photons·m^{-2}·s^{-1} at the surface of the mesocosms at midday and following the equation $I_{mix} = I_0(1 - e^{-kz})(kz)^{-1}$ (40) with I_0 being the incident light intensity at the surface, a typical winter water light attenuation coefficient $k = 0.25\ m^{-1}$ (41), and a water depth of $z = 1$ m, a mean daily photon flux of 1.93 mol photons·m^{-2}·d^{-1} was calculated.

ACKNOWLEDGMENTS. We thank Andrea Ludwig and Peter Fritsche for technical assistance during and after the experiment and for the elemental and carbohydrate analyses, Michael Meyerhöfer for DIC measurements, Hergen Johannsen for analysis of dissolved inorganic nutrients, Kai G. Schulz for help with the correction of DIC data for air-sea gas exchange, and Nicole Händel for help with the analysis of carbohydrates. This work was supported by the Deutsche Forschungsgemeinschaft as part of priority program 1162 AQUASHIFT.

1. Barnett TP, et al. (2005) Penetration of human-induced warming into the world's oceans. *Science* 309:284–287.
2. Sabine CL, et al. (2004) The oceanic sink for anthropogenic CO_2. *Science* 305:367–371.
3. Levitus S, Antonov J, Boyer T (2005) Warming of the world ocean 1955–2003. *Geophys Res Lett*, 10.1029/2004GL021592.
4. Bindoff NL, et al. (2007) in *Climate Change 2007: The Physical Science Basis*, eds Solomon S, et al. (Cambridge Univ Press, Cambridge, UK), pp 386–432.
5. Meehl GA, et al. (2007) in *Climate Change 2007: The Physical Science Basis*, eds Solomon S, et al. (Cambridge Univ Press, Cambridge, UK), pp 748–845.
6. Eppley RW (1972) Temperature and phytoplankton growth in the sea. *Fish Bull* 70:1063–1085.
7. Pomeroy LR, Wiebe WJ (2001) Temperature and substrates as interactive limiting factors for marine heterotrophic bacteria. *Aquat Microb Ecol* 23:187–204.
8. Rivkin RB, Legendre L (2001) Biogenic carbon cycling in the upper ocean: Effects of microbial respiration. *Science* 291:2398–2400.
9. Claquin P, Probert I, Lefebvre S, Veron B (2008) Effects of temperature on photosynthetic parameters and TEP production in eight species of marine microalgae. *Aquat Microb Ecol* 51:1–11.
10. Thornton DCO, Thake B (1998) Effect of temperature on the aggregation of *Skeletonema costatum* (Bacillariophyceae) and the implication for carbon flux in coastal waters. *Mar Ecol Prog Ser* 174:223–231.
11. Passow U, Alldredge AL (1995) Aggregation of a diatom bloom in a mesocosm: The role of transparent exopolymer particles (TEP). *Deep-Sea Res* II 42:99–109.
12. Engel A (2004) Distribution of transparent exopolymer particles (TEP) in the northeast Atlantic Ocean and their potential significance for aggregation processes. *Deep-Sea Res I* 51:83–92.
13. Thingstad TF, Hagstrom A, Rassoulzadegan F (1997) Accumulation of degradable DOC in surface waters: Is it caused by a malfunctioning microbial loop? *Limnol Oceanogr* 42:398–404.
14. Azam F (1998) Microbial control of oceanic carbon flux: The plot thickens. *Science* 280:694–696.
15. Laws EA, Falkowski PG, Smith WO, Jr, Ducklow H, McCarthy JJ (2000) Temperature effects on export production in the open ocean. *Glob Biogeochem Cycles* 14:1231–1246.
16. Riebesell U, et al. (2000) Reduced calcification of marine plankton in response to increased atmospheric CO_2. *Nature* 407:364–367.
17. Orr JC, et al. (2005) Anthropogenic ocean acidification over the 21st century and its impact on calcifying organisms. *Nature* 437:681–686.
18. Bijma J, Spero HJ, Lea DW (1999) in *Use of Proxies in Paleoceanography: Examples from the South Atlantic*, eds Fisher G, Wefers G (Springer, New York), pp 489–512.
19. Riebesell U, et al. (2007) Enhanced biological carbon consumption in a high CO_2 ocean. *Nature* 450:545–549.
20. Beaugrand G, Reid PC, Ibanez F, Lindley JA, Edwards M (2002) Reorganization of North Atlantic marine copepod biodiversity and climate. *Science* 296:1692–1694.
21. Perry AL, Low PJ, Ellis JR, Reynolds JD (2005) Climate change and distribution shifts in marine fishes. *Science* 308:1912–1915.
22. Pörtner HO, Knust R (2007) Climate change affects marine fishes through the oxygen limitation of thermal tolerance. *Science* 315:95–97.

23. Paerl HW, Huisman J (2008) Blooms like it hot. *Science* 320:57–58.
24. Edwards M, Richardson AJ (2004) Impact of climate change on marine pelagic phenology and trophic mismatch. *Nature* 430:881–884.
25. Beaugrand G, Brander KM, Lindley JA, Souissi S, Reid PC (2003) Plankton effect on cod recruitment in the North Sea. *Nature* 426:661–664.
26. Giorgi F, et al. (2001) in *Climate Change 2001: The Scientific Basis*, eds Houghton JT, et al. (Cambridge Univ Press, Cambridge, UK), pp 585–638.
27. Siegel DA, Doney SC, Yoder JA (2002) The North Atlantic spring phytoplankton bloom and Sverdrup's critical depth hypothesis. *Science* 296:730–733.
28. Hansen HP, Koroleff F (1999) in *Methods of Seawater Analysis*, eds Grasshoff K, Kremling K, Ehrhardt M (Wiley, Weinheim, Germany), pp 159–228.
29. Holmes RM, Aminot A, Kérouel R, Hooker BA, Peterson BJ (1999) A simple and precise method for measuring ammonium in marine and freshwater ecosystems. *Can J Fish Aquat Sci* 56:1801–1808.
30. Johnson KM, Sieburth JM, Williams PJ, Brändström L (1987) Coulometric total carbon dioxide analysis for marine studies: Automation and calibration. *Mar Chem* 21:117–133.
31. Gran G (1952) Determination of the equivalence point in potentiometric titrations of seawater with hydrochloric acid. *Oceanol Acta* 5:209–218.
32. Welschmeyer NA (1994) Fluorometric analysis of chlorophyll a in the presence of chlorophyll b and pheopigments. *Limnol Oceanogr* 39:1985–1992.
33. Sharp JH (1974) Improved analysis for ''particulate'' organic carbon and nitrogen from seawater. *Limnol Oceanogr* 19:984–989.
34. Qian J, Mopper K (1996) Automated high-performance, high-temperature combustion total organic carbon analyzer. *Anal Chem* 68:3090–3097.
35. Simon M, Azam F (1989) Protein content and protein synthesis rates of planktonic marine bacteria. *Mar Ecol Prog Ser* 51:201–213.
36. Fuhrman JA, Azam F (1982) Thymidine incorporation as a measure of heterotrophic bacterioplankton production in marine surface waters: Evaluation and field results. *Mar Biol* 66:109–120.
37. Gocke K, Hoppe HG (1977) in *Microbial Ecology of a Brackish Water Environment*, ed Rheinheimer G (Springer, Berlin), pp 61–70.
38. Delille B, et al. (2005) Response of primary production and calcification to changes of pCO_2 during experimental blooms of the coccolithophorid *Emiliania huxleyi. Global Biogeochem Cycles*, 10.1029/2004GB002318.
39. Kuss J, Schneider B (2004) Chemical enhancement of the CO_2 gas exchange at a smooth seawater surface. *Mar Chem* 91:165–174.
40. Riley GA (1957) Phytoplankton of the North Central Sargasso Sea. *Limnol Oceanogr* 2:252–270.
41. Sommer U, Lengfellner K (2008) Climate change and the timing, magnitude, and composition of the phytoplankton spring bloom. *Glob Change Biol* 14:1199–1208.